

Carbon supported manganese(IV)–cobalt(II/III) oxides nanoparticles for high-performance electrochemical supercapacitors

Jolita Jablonskienė*

Dijana Šimkūnaitė,

Jūratė Vaičiūnienė,

Giedrius Stalnionis,

Audrius Drabavičius,

Loreta Tamašauskaitė-Tamašiūnaitė,

Eugenijus Norkus

*Center for Physical Sciences
and Technology,
3 Saulėtekio Avenue,
10257 Vilnius, Lithuania*

The carbon supported manganese(IV)–cobalt (II/III) oxides nanoparticles labelled as $\text{MnO}_2\text{-Co}_3\text{O}_4/\text{C}$ nanocomposites have been prepared by a simple one-step microwave-assisted heating method using different precursor materials. Scanning electron microscopy (SEM), transmission electron microscopy (TEM) and inductively coupled plasma optical emission spectroscopy (ICP-OES) have been used for the characterization of morphology, structure and composition of the synthesized nanocomposites, whereas the electrochemical performance of the prepared nanocomposites has been evaluated by using cyclic voltammetry (CV).

It was determined that the use of different precursor materials for the synthesis of the carbon supported MnO_2 and Co_3O_4 nanocomposites results in a different morphology of the prepared substances. A high specific capacitance (C_s) of 658.8 F g^{-1} at a scan rate of 10 mV s^{-1} in a $1 \text{ M Na}_2\text{SO}_4$ solution has been obtained for the $\text{MnO}_2\text{-Co}_3\text{O}_4/\text{C-2}$ nanocomposite that has a spherical shape of nanoparticles. Moreover, it significantly outperforms the $\text{MnO}_2\text{-Co}_3\text{O}_4/\text{C-1}$ nanocomposite that has a lamellar shape of nanoparticles.

Keywords: manganese, cobalt, carbon, nanocomposites, supercapacitors

INTRODUCTION

Supercapacitors (SCs) have gained increasing attention due to their high power density, long cycle life, fast charge/discharge rate, and in recent years are seriously viewed as potential candidates of next-generation energy storage devices [1, 2]. They are especially valued for lightness and flexibility determining their large-scale of possible applications ranging from consumer electronic or portable devices like mobile phones, computers and memory back-up systems to hybrid electric vehicles or even

large industrial machinery, for defense and military or space equipment [3, 4].

The key issues in the commercial success of SCs application are directly linked to the selection and fabrication of the new, low-cost and efficient electrode materials offering a high potential for the substantially enhanced energy densities [3, 5]. Based on different energy storage principles, supercapacitors are generally categorized into electrochemical double-layer capacitors that use large surface-area carbon materials [6–8] and pseudocapacitors that use transition metal oxides (TMOs) as active materials. Among the emerging electrode materials for pseudocapacitors,

* Corresponding author. Email: jolita.jablonskiene@ftmc.lt

nanoscaled or mixed TMOs such as RuO_2 , MnO_2 , Co_3O_4 , NiO , Fe_3O_4 and V_2O_5 are the most attractive materials for their high theoretical specific capacitances (C_s), originating from fast and reversible redox reactions with the electrolyte ions [3].

Nevertheless, Ru-based materials dominate. They are most extensively explored due to the ultrahigh theoretical specific capacitance of RuO_2 (reaching over 1300 F g^{-1}), exceptional properties, including metallic-type conductivity, wide potential window and highly reversible redox reaction [9, 10]. But the relatively high cost, toxicity and limited environmental distribution of RuO_2 restrict its large-scale commercial application in SCs. On the contrary, TMOs, specially Co_3O_4 [11–13] and MnO_2 [14, 15] are considered rather promising electrode materials for SCs, since both of them are low priced, abundant, environment-friendly materials that are rich in oxidation states for efficient charge transfer, have various morphologies and exceptionally high theoretical specific capacitances (C_s) of 3560 or 1370 F g^{-1} , respectively. However, regardless the fascinating characteristics typically TMOs suffer from their low actual specific capacitance due to poor conductivity and electrochemical stability, low contacting area with the electrolytes and structural degradation during the charge-discharge process [16, 17]. In order to improve the capacitive performance of TMOs nanostructured electrode material with various morphologies that have a high specific surface area and a large surface-to-volume ratio for more effective contact with electrolyte ions, such as mesoporous MnO_2 nanotubes/nanosheets [18], nanowires [19] or flower-like, urchin-like and nanorod-like structures [20] or ultra-small Co_3O_4 nanocubes [21], hollow coral-shaped nanostructures [12] or nanosheets [22] have been created. Incorporation of foreign conductive metals including Au, Al, Cu, Fe, Mg and Co [23–30] into TMOs lattices has been successfully applied and revealed the increase in C_s , for example, in the presence of Co the achieved C_s value was of 350 F g^{-1} at a current density of 0.1 A g^{-1} [29]. Analogously, creating binary, ternary or multy-mixed TMOs allowed improving the capacitive performance of those electrode materials, compared to that of the single metal compounds [31–35]. Among them, for example, are ultrathin amorphous Co-Fe-B nanosheets

deposited on the 3-dimensional nickel foam substrate with C_s of ca. 981 F g^{-1} at 1 A g^{-1} [31]; Mn-Co-Fe ternary hydroxide nanoplatelets directly settled on Ni foam delivering the maximum C_s of 1200 F g^{-1} at a scan rate of 5 mV s^{-1} [32]; the $\text{Co}_3\text{O}_4@\text{PPy}@\text{MnO}_2$ ‘core-shell-shell’ nanowire arrays on the nickel foam substrate exhibited a prominent electrochemical performance with a high energy density of 34.3 Wh kg^{-1} at a power density of 80.0 W kg^{-1} [33]; $\text{MnO}_2/\text{Ni}(\text{OH})_2/\text{NF}$ composite with high C_s of 506 F g^{-1} at 16.7 A g^{-1} [34]; tremella-like $\text{NiO}@\text{Co}_3\text{O}_4@\text{MnO}_2$ particles offered high C_s of 792.6 F g^{-1} at 2 A g^{-1} [35]. The flower-like $\text{Co}_3\text{O}_4@\text{MnO}_2$ core-shell microspheres coated on nickel foam exhibited a significantly enhanced C_s of 671 F g^{-1} at 1 A g^{-1} [36]. Furthermore, in order to overcome the above-mentioned drawbacks, combining TMOs with high conductive substrates such as graphene, porous carbon, carbon nanotubes, activated carbon or carbon fiber is regarded not only an effective way to improve the electrochemical performance of SCs, but makes those materials rather attractive for fabricating flexible electrode materials with the aim to apply them as flexible, light and inexpensive energy storage devices. Recently, due to the synergic effect Co- Co_3O_4 @carbon-nanotube (CNT)-incorporated N-doped carbon (C_s of 671 F g^{-1} at 1 A g^{-1}) [37] or in situ fabricated MnO_2 and its derived FeOOH nanostructures on mesoporous carbon [38] further enhance the electrochemical performance of those TMOs structures and showed a great potential in application for energy storage devices. The core-shell nanostructured TMOs have shown to be more stable, and able for providing an outstanding cycling stability at a high current density. Among them are the hierarchical core-shell $\text{NiCo}_2\text{O}_4@\text{NiMoO}_4$ nanowires grown on carbon cloth [39] or manganese-nickel-cobalt sulfide (MNCS) multi-tripod nanotube arrays (NTAs) on a carbon nanotube fibers (CNTFs) surface [40], which could serve as flexible binder-free electrode materials for supercapacitors.

Herein, we demonstrate a facile microwave-assisted heating method for the synthesis of carbon supported MnO_2 - Co_3O_4 nanocomposites using different precursor materials with the aim to apply them as material for electrochemical supercapacitors.

EXPERIMENTAL

Preparation of nanocomposites

The $\text{MnO}_2\text{-Co}_3\text{O}_4$ nanocomposite supported on carbon was prepared in two different ways by the microwave-assisted heating. In the first way, 0.2 g of KMnO_4 , 0.737 g of $\text{Co}(\text{NO}_3)_2\cdot 7\text{H}_2\text{O}$ and 0.1 g of carbon powder were dispersed in 20 ml of deionized water. The obtained reaction mixture was put into a microwave reactor Monowave 300 (Anton Paar) for 5 min at 150°C temperature. The precipitate was filtered out, washed with water and dried in a vacuum oven at 80°C temperature for 4 h. The prepared nanocomposite was labelled as $\text{MnO}_2\text{-Co}_3\text{O}_4/\text{C-1}$. In the second way, 0.2 g of KMnO_4 , 0.01 g of Co_3O_4 and 0.1 g of carbon powder were dispersed in 20 ml of deionized water. The synthesis of nanocomposite was carried out at the same conditions. The prepared nanocomposite was labelled as $\text{MnO}_2\text{-Co}_3\text{O}_4/\text{C-2}$. Notably, Co_3O_4 was prepared by annealing of $\text{Co}(\text{NO}_3)_2\cdot 7\text{H}_2\text{O}$ in air atmosphere in a muffle furnace at 400°C temperature. The formation of pure Co_3O_4 was confirmed by XRD analysis (not shown).

For comparison, the carbon supported Co_3O_4 nanocomposite labelled as $\text{Co}_3\text{O}_4/\text{C}$ was prepared by mixing 0.01 g of Co_3O_4 and 0.1 g of carbon powder in 20 ml of deionized water. The synthesis of nanocomposite was also carried out at the same conditions.

Characterization of nanocomposites

The morphology and composition of the prepared catalysts were characterized using a SEM-focused ion beam facility (Helios Nanolab 650) equipped with an EDX spectrometer (INCA Energy 350 X-Max 20). A shape and size of catalyst particles were examined using a transmission electron microscope Tecnai G2 F20 X-TWIN equipped with an EDX spectrometer with an r-TEM detector. For microscopic examinations, 10 mg of the sample was first sonicated in 1 ml of ethanol for 1 h and then deposited on the Ni grid covered with a continuous carbon film. Mn and Co loadings in the prepared samples were estimated using an ICP optical emission spectrometer Optima 7000DV (Perkin Elmer).

Electrochemical measurements

The electrochemical performance of $\text{MnO}_2\text{-Co}_3\text{O}_4/\text{C}$ and $\text{Co}_3\text{O}_4/\text{C}$ nanocomposites was tested using

a Zennium electrochemical workstation (ZAHNER-Elektrik GmbH & Co. KG). The prepared nanocomposites coated on the glassy carbon electrode (GCE) with a geometric surface area of 0.07 cm^2 were employed as a working electrode, a Pt sheet as a counter electrode, and an $\text{Ag}/\text{AgCl}/\text{KCl}$ electrode was used as a reference. The working electrodes were prepared as follows: 10 mg of the prepared nanocomposites were dispersed ultrasonically in 0.1 ml of 2% of polyvinylidene fluoride (PVDF) in an N-methyl-2-pyrrolidinone (NMP) solution for 1 h. Then, 5 μL of the prepared suspension mixture was pipetted onto the polished surface of GCE and dried in an oven for 2 h at 80°C .

Cyclic voltammograms (CVs) were recorded in a 1 M Na_2SO_4 solution at different scan rates between 10 and 200 mV s^{-1} at ambient temperature. The measuring potential range was from 0.05 to 1.10 V. All solutions were deaerated by argon for 15 min prior to measurements.

RESULTS AND DISCUSSION

The surface morphology of the prepared $\text{MnO}_2\text{-Co}_3\text{O}_4/\text{C}$ nanocomposites was investigated by SEM analyses. Figure 1 shows the SEM images of $\text{MnO}_2\text{-Co}_3\text{O}_4/\text{C-1}$ (a, b) and $\text{MnO}_2\text{-Co}_3\text{O}_4/\text{C-2}$ (c, d) under different magnification. The use of different precursor materials for the synthesis of the carbon supported MnO_2 and Co_3O_4 nanocomposites results in a different morphology of the prepared ones. As evident from Fig. 1a and b, the $\text{MnO}_2\text{-Co}_3\text{O}_4/\text{C-1}$ nanocomposite has a spatial layer of irregularly shaped lamellar nanostructures of ca. 10–50 nm in size. Meanwhile, in the case of $\text{MnO}_2\text{-Co}_3\text{O}_4/\text{C-2}$ nanocomposite, the spongy and porous frost-like three-dimensional surface is observed (Fig. 1c, d). The widely sprayed branches range from several to hundred nm in size.

More detailed microstructural information of the synthesized $\text{MnO}_2\text{-Co}_3\text{O}_4/\text{C}$ nanocomposites has been provided by TEM analysis and are shown in Fig. 1e–h. The obtained data are in line with those determined by SEM analysis. In the case of $\text{MnO}_2\text{-Co}_3\text{O}_4/\text{C-1}$ nanocomposite, tapered nanowires and nanosheets are almost uniformly distributed on the surface (Fig. 1e, f). Moreover, the aggregated spherical nanostructures composed of oblong branches are seen in the prepared $\text{MnO}_2\text{-Co}_3\text{O}_4/\text{C-2}$ nanocomposite (Fig. 1g, h).

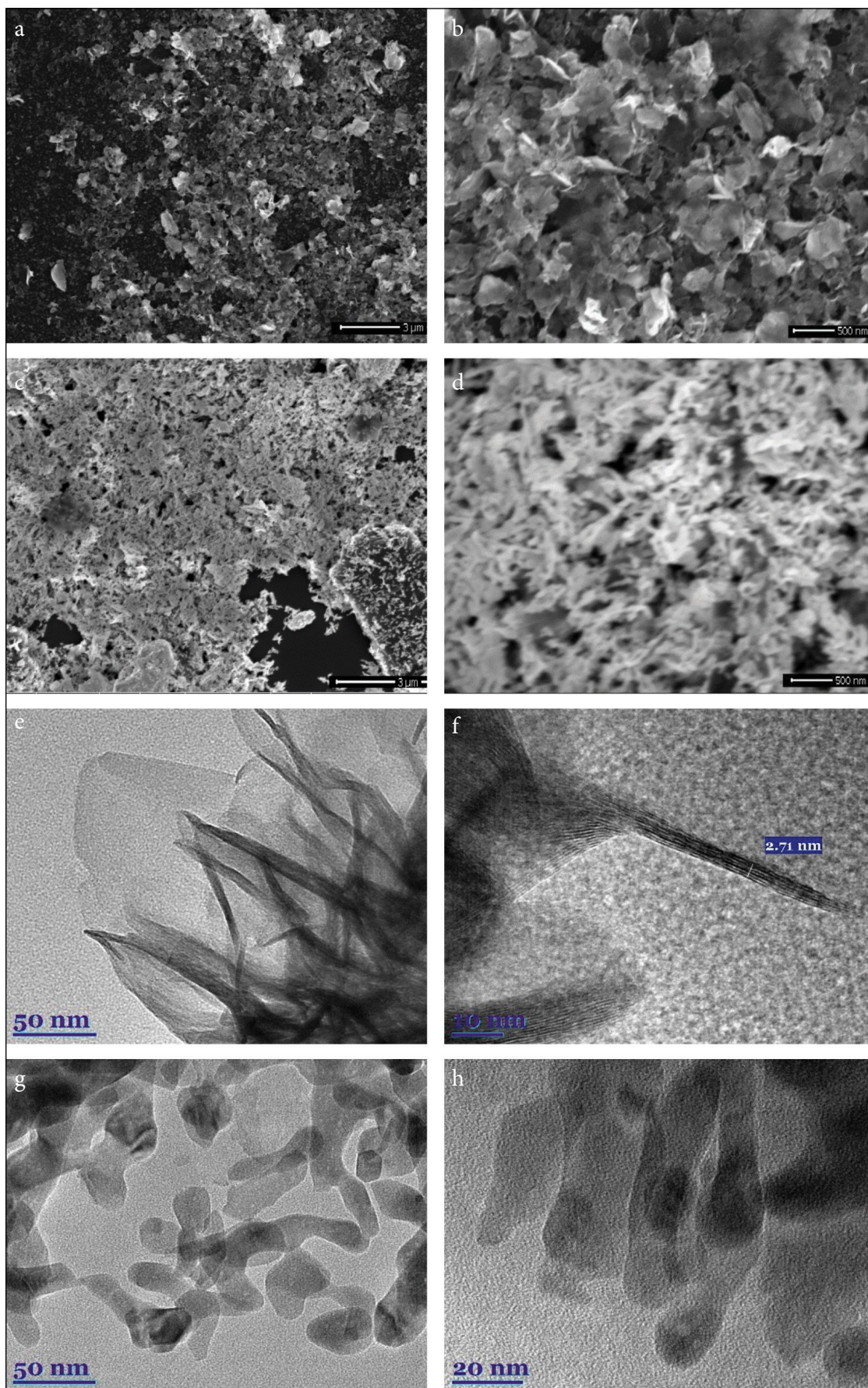


Fig. 1. SEM and TEM images of MnO₂-Co₃O₄/C-1 (a, b, e, f) and MnO₂-Co₃O₄/C-2 (c, d, g, h) under different magnifications

The electrochemical performance of the $\text{MnO}_2\text{-Co}_3\text{O}_4/\text{C}$ nanocomposites was evaluated from the cyclic voltammetry using a three-electrode system in an aqueous 1 M Na_2SO_4 electrolyte. Figure 2 presents the CVs of $\text{MnO}_2\text{-Co}_3\text{O}_4/\text{C-1}$ (a), $\text{MnO}_2\text{-Co}_3\text{O}_4/\text{C-2}$ (b) and $\text{Co}_3\text{O}_4/\text{C}$ (c) at scan rates of 10, 50, 100 and 200 mV s^{-1} in a potential window of 0.05 to 1.1 V vs SHE. The CVs of all the nanocomposites at a scan rate of 10 mV s^{-1} are shown in Fig. 2d. As evident, the all prepared nanocomposites show a quasi-rectangular and symmetric voltammetry curves at a low scan rate, indicating their good capacitive behaviour (Fig. 2d). Notably, with increasing scan rate up to 200 mV s^{-1} , the current density values increase gradually, but CVs do not always maintain a rectangular shape, especially at a high scan rate (Fig. 2a–c). The CV area of $\text{MnO}_2\text{-Co}_3\text{O}_4/\text{C-2}$ nanocomposite is larger than

that of $\text{MnO}_2\text{-Co}_3\text{O}_4/\text{C-1}$ and $\text{Co}_3\text{O}_4/\text{C}$ (Fig. 2d). This result suggests that the specific capacitance of $\text{MnO}_2\text{-Co}_3\text{O}_4/\text{C-2}$ nanocomposite is higher as compared with that for $\text{MnO}_2\text{-Co}_3\text{O}_4/\text{C-1}$ and $\text{Co}_3\text{O}_4/\text{C}$ nanocomposites. C_s (F g^{-1}) of the electrode material was calculated from the CV test according to the following equation (Eq. 1) [41]:

$$C_s = \frac{1}{m \cdot \nu \cdot \Delta V} \int i dv. \quad (1)$$

Here C_s is the specific capacitance (F g^{-1}), m is the mass of the active material (g), ν is the scan rate of potential (V s^{-1}), ΔV is the range of scan potential (V), and i is the current (A). Plots of C_s versus scan rate for $\text{MnO}_2\text{-Co}_3\text{O}_4/\text{C-1}$, $\text{MnO}_2\text{-Co}_3\text{O}_4/\text{C-2}$ and $\text{Co}_3\text{O}_4/\text{C}$ are presented in Fig. 3. It is clearly seen that the C_s values of all the nanocomposites decrease with the growth of scan rate from 10 to 200 mV s^{-1} ,

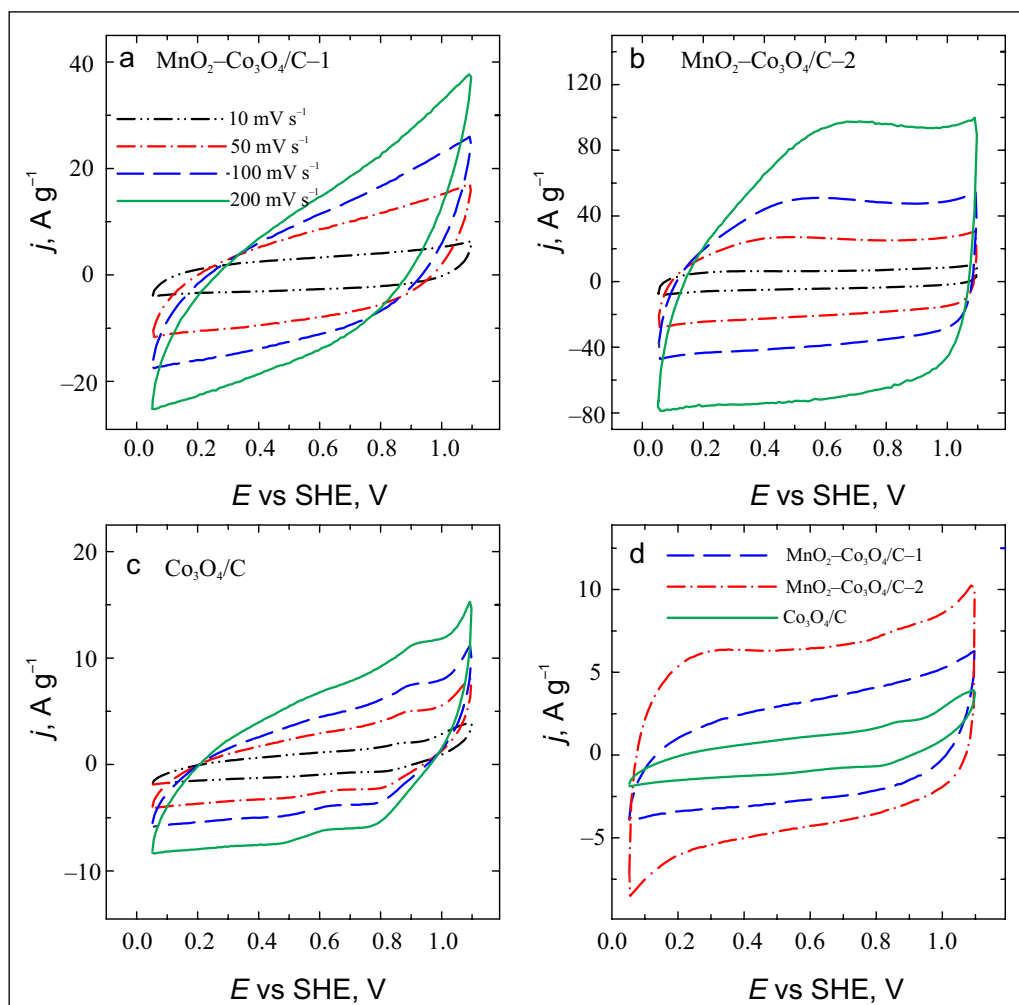


Fig. 2. CVs of $\text{MnO}_2\text{-Co}_3\text{O}_4/\text{C-1}$ (a), $\text{MnO}_2\text{-Co}_3\text{O}_4/\text{C-2}$ (b) and $\text{Co}_3\text{O}_4/\text{C}$ (c). (d) CVs of the same nanocomposites at a scan rate of 10 mV s^{-1}

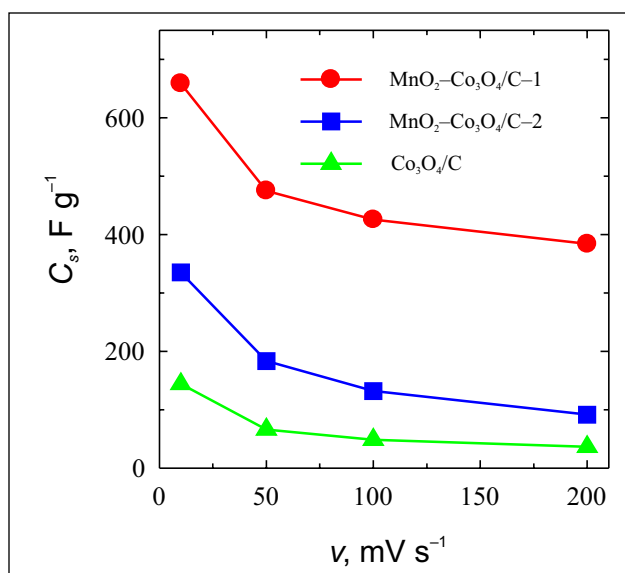


Fig. 3. Plots of the specific capacitance versus scan rate of $\text{MnO}_2\text{-Co}_3\text{O}_4/\text{C-1}$, $\text{MnO}_2\text{-Co}_3\text{O}_4/\text{C-2}$ and $\text{Co}_3\text{O}_4/\text{C}$ nanocomposites

nevertheless the C_s values of the nanocomposites are still higher. The calculated C_s value for the $\text{MnO}_2\text{-Co}_3\text{O}_4/\text{C-2}$ nanocomposite is highest at a scan rate of 10 mV s^{-1} among the investigated nanocomposites and equal to 658.8 F g^{-1} (Fig. 3). This value is much larger than that of $\text{MnO}_2\text{-Co}_3\text{O}_4/\text{C-1}$ (335.0 F g^{-1}) and pure $\text{Co}_3\text{O}_4/\text{C}$ (144.1 F g^{-1}). When the scan rate increases to 200 mV s^{-1} , the $\text{MnO}_2\text{-Co}_3\text{O}_4/\text{C-1}$, $\text{MnO}_2\text{-Co}_3\text{O}_4/\text{C-2}$ and $\text{Co}_3\text{O}_4/\text{C}$ nanocomposites still exhibit C_s of 91.6 , 384.2 and 36.7 F g^{-1} , respectively (Fig. 3). The $\text{MnO}_2\text{-Co}_3\text{O}_4/\text{C-1}$, $\text{MnO}_2\text{-Co}_3\text{O}_4/\text{C-2}$ and $\text{Co}_3\text{O}_4/\text{C}$ nanocomposites preserve 27.3 , 58.3 and

25.5% , respectively, of their specific capacitance (from 335.0 F g^{-1} to 91.6 F g^{-1} , from 658.8 F g^{-1} to 384.2 F g^{-1} , and from 144.1 F g^{-1} to 36.7 F g^{-1}) as the scan rate increases from 10 mV s^{-1} to 200 mV s^{-1} .

Comparison of the supercapacitive behaviour of MnO_2 nanocomposites reported in literature and the present work are listed in the Table, exhibiting the high specific capacitance of our prepared electrode materials.

CONCLUSIONS

In this study, we report a rapid synthesis of the carbon supported MnO_2 and Co_3O_4 nanocomposites via a simple and facile microwave-assisted heating method without any complicated extra-post-treatment procedures. The application of different precursor materials for the preparation of carbon supported $\text{MnO}_2\text{-Co}_3\text{O}_4$ determines directly the formation of nanocomposites having different morphology such as irregularly shaped lamellar or spherical nanostructures that have a decisive impact on the electrochemical performance. The highest specific capacitance of 658.8 F g^{-1} at a scan rate of 10 mV s^{-1} has been achieved at the $\text{MnO}_2\text{-Co}_3\text{O}_4/\text{C-2}$ nanocomposite that has a spherically shaped nanoparticle architecture in comparison with that of $\text{MnO}_2\text{-Co}_3\text{O}_4/\text{C-1}$ with a lamellar shape structure. The prepared $\text{MnO}_2\text{-Co}_3\text{O}_4$ nanocomposites are expected to be a promising electrode material for supercapacitor applications.

Table. Comparison of C_s for various MnO_2 -based electrode materials

Materials	Scan rate, current density	Specific capacitance, F g^{-1}	Ref.
$\text{MnO}_2\text{-Co}_3\text{O}_4/\text{C-1}$	10 mV s^{-1}	335.0	This work
$\text{MnO}_2\text{-Co}_3\text{O}_4/\text{C-2}$	10 mV s^{-1}	658.8	This work
Co-doped MnO_2	10 mV s^{-1}	287.0	[29]
$\text{Co}_3\text{O}_4@\text{PPy}@\text{MnO}_2$	2 mV s^{-1}	518.0	[33]
Biomorphic Co_3O_4 nanocrystal/mesoporous carbon microtube composites	1 A g^{-1}	284.2	[11]
Hollow coral-shaped Co_3O_4 nanostructures	5 mV s^{-1}	626.5	[12]
Co_3O_4 core-shell microspheres	0.5 A g^{-1}	261.1	[13]
Au-doped MnO_2	5 mV s^{-1}	626.0	[24]
Cobalt-doped MnO_2 hierarchical yolk-shell spheres	0.1 A g^{-1}	350	[29]
Flower-like $\text{Co}_3\text{O}_4@\text{MnO}_2$ core-shell composite	1 A g^{-1}	671	[36]

ACKNOWLEDGEMENTS

This research is funded by the European Social Fund under Measure No. 09.3.3-LMT-K-712-02-0142 'Development of Competences of Scientists, other Researchers and Students through Practical Research Activities'.

Received 17 March 2020

Accepted 19 March 2020

References

1. F. Wang, X. Wu, X. Yuan, et al., *Chem. Soc. Rev.*, **46**, 6854 (2017).
2. C. Liu, X. Yan, F. Hu, et al., *Adv. Mater.*, **30**, 1705713 (2018).
3. Poonam, K. Sharma, A. Arora, S. K. Tripathi, *J. Energy Storage*, **21**, 825 (2019).
4. C. V. V. Muralee Gopi, R. Vinodh, S. Sambasivam, et al., *J. Energy Storage*, **27**, 101035 (2020).
5. G. Wang, L. Zhang, J. Zhang, *Chem. Soc. Rev.*, **41**, 797 (2012).
6. L. L. Liu, Z. Q. Niu, J. Chen, *Chem. Soc. Rev.*, **45**, 4363 (2016).
7. K. Bazaka, M. V. Jacob, K. Ostrikov, *Chem. Rev.* **116**, 214 (2016).
8. F. Lai, Y. E. Miao, L. Zuo, et al., *Small*, **12**, 3199 (2016).
9. A. Muzaffar, M. Basheer Ahamed, K. Deshmukha, et al., *Renew. Sustain. Energy Rev.* **101**, 145 (2019).
10. A. Afif, S. M. H. Rahman, A. T. Azad, et al., *J. Energy Storage*, **25**, 100852 (2019).
11. D. Sun, L. Hea, R. Chen, et al., *Appl. Surf. Sci.* **465**, 240 (2019).
12. X. Wang, N. Zhang, X. Chen, et al., *Colloids Surf. A*, **570**, 72 (2019).
13. D. Guo, X. Song, F. Li, et al., *Colloids Surf. A*, **546**, 8 (2018).
14. W. Guo, C. Yu, S. Li, et al., *Nano Energy*, **57**, 472 (2019).
15. J.-G. Wang, F. Kang, B. Wei, *Prog. Mater. Sci.*, **74**, 124 (2015).
16. C. D. Lokhande, D. P. Dubal, O.-S. Joo, *Curr. Appl. Phys.*, **11**, 270 (2011).
17. X. Guo, G. Zhang, Q. Li, et al., *Energy Stor. Mater.*, **15**, 201 (2018).
18. M. Huang, Y. Zhang, F. Li, et al., *Sci. Rep.*, **4**, 3886 (2014).
19. B. Yin, S. Zhang, Y. Jiao, et al., *Cryst Eng Comm.*, **16**, 10005 (2014).
20. J. Chu, D. Lu, J. Ma, et al., *Mater. Lett.*, **193**, 265 (2017).
21. M. Pal, R. Rakshit, A. K. Singh, et al., *Energy*, **103**, 486 (2016).
22. X. Pan, X. Chen, Y. Li, et al., *Electrochim. Acta*, **182**, 1106 (2015).
23. Q. Lv, H. Sun, X. Li, et al., *Nano Energy*, **21**, 50 (2016).
24. J. Kang, A. Hirata, L. Kang, et al., *Chem. Int. Ed.*, **52**, 1667 (2013).
25. Z. M. Hu, X. Xiao, C. Chen, et al., *Nano Energy*, **11**, 234 (2015).
26. X. Su, L. Yu, G. Cheng, et al., *Appl. Energy*, **134**, 445 (2014).
27. R. Peng, N. Wu, Y. Zheng, et al., *ACS Appl. Mater. Interf.*, **8**, 8480 (2016).
28. Z. Wang, F. Wang, Y. Li, et al., *Nanoscale*, **8**, 7317 (2016).
29. C.-L. Tang, X. Wei, Y.-M. Jiang, et al., *J. Phys. Chem. C.*, **119**, 8471 (2015).
30. A. M. Hashem, H. M. Abuzeid, N. Narayanan, et al., *Mater. Chem. Phys.*, **130**, 38 (2011).
31. Q. Meng, W. Xu, S. Zhu, et al., *Electrochim. Acta*, **296**, 205 (2019).
32. A. E. Elkholy, F. El-Taib Heakal, N. K. Allam, *Electrochim. Acta*, **296**, 68 (2019).
33. L. Han, P. Tang, L. Zhang, *Nano Energy*, **7**, 51 (2014).
34. F. Wang, Q. Zhou, G. Li, et al., *J. Alloys Compd.*, **700**, 190 (2017).
35. H. Wang, Q. Ren, J. L. Brett Dan, et al., *J. Power Sources*, **343**, 82 (2017).
36. H. Che, Y. Lv, A. Liu, et al., *Ceram. Int.*, **43**, 6062 (2017).
37. Y. Zou, C. Cai, C. Xiang, et al., *Electrochim. Acta*, **261**, 547 (2018).
38. Y. Chen, C. Jing, X. Fu, et al., *Appl. Surf. Sci.*, **503**, 144123 (2020).
39. L. Huang, W. Zhang, J. Xiang, et al., *Sci. Rep.*, **6**, 31465 (2016).
40. X. Wang, Q. Zhang, J. Sun, et al., *J. Mater. Chem. A*, **6**, 8038 (2018).
41. X. Meng, L. Lu, C. Sun, *ACS Appl. Mater. Interf.*, **10**, 16481 (2018).

**Jolita Jablonskienė, Dijana Šimkūnaitė,
Jūratė Vaičiūnienė, Giedrius Stalnionis,
Audrius Drabavičius,
Loreta Tamašauskaitė-Tamašiūnaitė,
Eugenijus Norkus**

**MANGANO(IV)-KOBALTO(II/III) OKSIDŲ,
SUFORMUOTŲ ANT ANGLIES PAGRINDO,
TAIKYMAS ELEKTROCHEMINIAMS
SUPERKONDENSATORIAMS**

Santrauka

Naudojant iš skirtingų prekursorių susintetintus MnO_2 ir Co_3O_4 , $\text{MnO}_2\text{-Co}_3\text{O}_4/\text{C}$ nanokompozitai buvo formuojami ant anglies pagrindo taikant mikrobangų sintezės metodą. Skirtingais būdais suformuotų nanokompozitų morfologija ir sudėtis buvo tiriami naudojant skenuojančiąją elektronų mikroskopiją (SEM), peršviečiamąją elektroninę mikroskopiją (TEM) ir indukciškai susietos plazmos optinės emisijos spektroskopiją (ICP-OES). $\text{MnO}_2\text{-Co}_3\text{O}_4/\text{C}$ nanokompozitų elektrocheminė elgsena buvo tiriama taikant ciklinę voltamperometriją (CV).

Nustatyta, kad sintezės metu susidarančių nanokompozitų paviršiaus morfologija priklauso nuo naudotų prekursorių prigimties. Kai sintezėje buvo naudojamas Co_3O_4 , gaunamas $\text{MnO}_2\text{-Co}_3\text{O}_4/\text{C-2}$ nanokompozitas, kuriam yra būdingos sferinės formos nanodalelės. 1 M Na_2SO_4 tirpale, kai potencialo skleidimo greitis buvo 10 mV s^{-1} , išmatuotoji didžiausia specifinė talpa (C_s) vertė siekė $658,8 \text{ F g}^{-1}$. Be to, pastarasis nanokompozitas pasižymi žymiai geresnėmis katalizinėmis savybėmis nei $\text{MnO}_2\text{-Co}_3\text{O}_4/\text{C-1}$ nanokompozitas (šiuo atveju kaip prekursorius buvo naudojamas $\text{Co}(\text{NO}_3)_2$), kuriam būdingos plokštelinės formos nanodalelės.